Computational Simulation of Flows in Crystal Growth from Melts

B. C. Khoo D. Xu
(Centre for Computational Mechanics, National University of Singapore)
W. J. Ma*
(Institute of Mechanics, Chinese Academy of Sciences)

Abstract: *The numerical simulations of Czochralski and Bridgman crystal growth are performed and presented in the paper. The second order upwind QUICK scheme with finite control volume method is employed for the numerical calculations of melt flows in Czochralski crystal growth. It is found that the present calculation has much higher numerical accuracy and stability compared with other methods. The 3-dimensional time-dependent numerical calculations of melt flows in horizontal Bridgman crystal growth with high gravity by means of centrifuges shows that Coriolis force has stabilizing effect on the fluctuation of melt flows under specific rotation direction and rotation rate. The 3-dimensional numerical solutions agree with the experimental results, and are much more accurate than 2-dimensional numerical prediction.*

Introduction

Crystal growth from melts is a major way to produce a variety of materials for the manufacture of electronic and optical devices. During the process of growth, the flow of the melt plays a crucial role in determining the crystal quality. In most cases of crystal growth from melts the melt is at very high temperature and remains opaque, which makes it very difficult to observe the detailed structure of the associated flow field. With the rapid advancement of computer technology, CFD (Computational Fluid Dynamics) has become an increasing powerful and important tool for use to study the flow dynamics of the liquid phase and its influence on the crystal growth. Computational simulation enables the crystal growers to visualize the flow patterns and seek the optimal growth conditions with much resultant savings in terms of cost and time. In this article we present two examples of computational simulation of flows in crystal growth from melts performed at the Center for Computational Mechanics, National University of Singapore. The simulations involve some basic aspects of CFD and major configurations for crystal growth from melts.

Part I. Simulation of Steady Flows in Czochralski Crystal Growth

The Czochralski technique has been widely used to grow semiconductor and oxide crystals for decades, but the success to produce large size and good quality crystal depends very much on the experience and skill of the personnel involved. The modeling and understanding of heat and mass transfer have become an important issue in the optimization of the Czochralski technique to grow more uniform and better quality crystals. Several computer methods and models have been developed and are increasingly being used to simulate crystal growth in the

* currently works at National University of Singapore as a visiting scientist.

last decade[1-5]. The combination of natural convection due to thermal gradients between the crystal and crucible and forced convection due to rotation of the crystal and the crucible makes the problems very complex in terms of thermodynamics and hydrodynamics. With the increase of the heat conduction (Grashof number) and rotations of crystal or crucible (Reynolds number) as required in the Czochralski growth technique for the possible growth of a larger with less imperfection crystal, the convection term in the flow equations becomes much more dominant. This makes the second order central difference scheme unsuitable due to enhanced numerical instability. The motivation for the present study stems from the need to numerically simulate the flow in Czochralski crystal growth at more extreme conditions with higher order accuracy and using limited computing resources. In this respect, the Control Volume Method with the second order upwind QUICK scheme is used to simulate the fluid flow. The Wheeler's benchmark problem[6] is taken as the test example in Czochralski crystal growth.

Wheeler's Benchmark Problem

The Wheeler's benchmark problem for Czochralski crystal growth[6] is shown in Fig. 1. It consists essentially of a vertical cylindrical crucible of radius Rc filled with a melt to a height H and rotating with an angular velocity Ωc. The melt is bounded above by a coaxial crystal of radius $Rx < Rc$ rotating with angular velocity Ωx. The problem is solved subjected to the following assumptions:

- The free surface of the melt is flat and free of shear stress;
- The crystal is isothermal with temperature Tx;
- The side wall of crucible is isothermal with temperature Tc;
- The bottom of crucible is a perfect insulator;
- The temperature on the free surface of the melt assumes a linear distribution from Tx to Tc;
- The melt is an incompressible Newtonian Boussinesq fluid;
- The flow is axi-symmetric.

Mathematical Model

To Wheeler's problem, the non-dimensional governing equations (i. e. continuity, momentum and energy, equations) in the cylindrical coordinate system, can be written as:

$$\frac{1}{r}\frac{\partial (ru)}{\partial r}+\frac{\partial w}{\partial z}=0 \tag{1}$$

$$u\frac{\partial u}{\partial r}+w\frac{\partial u}{\partial z}-\frac{v^2}{r}=-\frac{\partial p}{\partial r}+\nabla^2 u-\frac{u}{r^2} \tag{2}$$

$$u\frac{\partial v}{\partial r}+w\frac{\partial v}{\partial z}+\frac{uv}{r}=\nabla^2 v-\frac{v}{r^2} \tag{3}$$

$$u\frac{\partial w}{\partial r}+w\frac{\partial w}{\partial z}=-\frac{\partial p}{\partial z}+\nabla^2 w+GrT \tag{4}$$

$$u\frac{\partial T}{\partial r}+w\frac{\partial T}{\partial z}=\frac{1}{Pr}\nabla^2 T \tag{5}$$

where $\nabla^2=\frac{1}{r}\frac{\partial}{\partial r}\left(r\frac{\partial}{\partial r}\right)+\frac{\partial^2}{\partial z^2}$

The boundary conditions are given by

$u=v=\frac{\partial w}{\partial r}=\frac{\partial T}{\partial r}=0$ for $r=0,\ 0\leqslant z\leqslant\alpha$;

$u=w=0,\ v=Re_c,\ T=1$ for $r=1,\ 0\leqslant z\leqslant\alpha$;

$$u=w=\frac{\partial T}{\partial z}=0,\quad v=rRe_c \qquad \text{for } 0\leqslant r\leqslant 1,\ z=0;$$

$$\frac{\partial u}{\partial z}=\frac{\partial v}{\partial z}=w=0,\quad T=\frac{(r-\beta)}{(1-\beta)} \qquad \text{for } \beta\leqslant r\leqslant 1,\ z=\alpha;$$

$$u=w=T=0,\quad v=rRe_x \qquad \text{for } 0\leqslant r\leqslant \beta,\ z=\alpha. \tag{6}$$

Here the non-dimensional parameters are the aspect ratios

$$\alpha=\frac{H}{R_c},\qquad \beta=\frac{R_x}{R_c}$$

the Reynolds numbers

$$Re_X=\frac{R_C^2\Omega_X}{\upsilon},\qquad Re_c=\frac{R_C^2\Omega_C}{\upsilon}$$

and the Prandtl and Grashof numbers

$$Pr=\frac{\upsilon}{\kappa},\qquad Gr=\frac{g\beta_t\ (T_C-T_X)\ R_C^3}{\upsilon^2}$$

where κ is the coefficient of thermal conductivity and β_t is the coefficient of volumetric expansion. In the present study, the aspect ratios and the Prandtl number are fixed at:

$$\alpha=1.0,\qquad \beta=0.4,\qquad Pr=0.05$$

Numerical Results and Discussion

The governing equations with their boundary conditions are numerically solved by using control volume method and the second order upwind QUICK scheme. The present solver is validated by the Wheeler' s benchmark problems. It is found that the present results agree very well with available data in the literature. However, the present solver can simulate the flow with much higher Grashof number.

The grid independence of the results is examined before the main calculations are carried out. The case A3, with $Gr=Re_C=0$, $Re_X=1.0\times10^4$, is repeatedly calculated with 5 kinds of grids from coarse to fine. The minimum and maximum values of stream function denoted by ψ_{min} and ψ_{max} respectively, and maximum velocity $|U|_{max}$ in the r-z plane are computed and compared for different grid sizes. From Table 1, a convergence to grid independence is fairly obvious. These computed results in turn are fairy comparable to the results of [2], which is listed in the last two columns in the Table 1. It may be said that for the most significant value of ψ_{min} the present solver has the same accuracy as the reference [2], which used the second, order central difference scheme to simulate the convection terms of Navier-Stokes equations.

To further validate the present solver, the numerical results of case A1, A2, and D2 (refer to table 4 for the meaning of case number) are compared with available data of [5] (See Table 2) which obtained the results using spectral multidomain method. It can be deduced that both calculations agree very well with $|U|_{max}$ and ψ_{min}. There are, however, some differences between ψ_{max} of present calculation and [5]'s calculation. Since the absolute value of ψ_{max} is very small, the difference can be considered to be negligible. Further comparison of these cases computed using the central difference scheme [2] has also indicated some differences in the numerical values of ψ_{min} and ψ_{max}. This is shown below in Table 3. However, in all these comparisons, there is very little difference in the stream function contours thereby indicating very similar flow features.

From the above, further computations pertaining to different flow conditions are carried out for the typical grid size of 80×80. It may be noted that morn grid lines are intensively distributed near to the solid wall of the crucible and the crystal to reflect the expected rapid change or much sharper gradient of flow field.

After validation of the present numerical solver, we calculated as many as 12 cases(classified under 4 groups) with different parameter sets(reflecting the associated flow conditions imposed)listed in Table 3.

Table 1 Grid Independence Test, Case A3, $Gr = 0$, $Re_X = 1.0 \times 10^4$, $Re_C = 0$

Mesh	$\lvert U\rvert^*_{max}$	ψ^*_{min}	ψ^*_{max}	ψ^{**}_{min}	ψ^{**}_{max}
20×20	833.97	-3.1515×10^1	1.7456×10^0	-3.2661×10^1	1.2563×10^{-1}
40×40	957.24	-3.9474×10^1	2.0885×10^{-3}	-4.1317×10^1	1.1625×10^{-1}
64×64	959.08	-4.0913×10^1	5.7303×10^{-2}	-4.0443×10^1	1.9320×10^{-1}
80×80	961.05	-4.1168×10^1	1.0443×10^{-1}	-4.2645×10^1	1.4583×10^{-1}
160×160	978.01	-4.2367×10^1	1.3366×10^{-1}	-4.2513×10^1	1.5918×10^{-1}
∞				-4.2419×10^1	1.6179×10^{-1}

* Present QUICK scheme; * * [2]'s central difference scheme.

Table 2 Some Results of Case A1, A2, D1 and D2

Case	$\lvert U\rvert^*_{max}$	ψ^*_{min}	ψ^*_{max}	$\lvert U\rvert^{**}_{max}$	ψ^{**}_{max}	ψ^{**}_{max}
A1	4.37	-2.17×10^{-1}	4.06×10^{-6}	4.46	-0.224	4.85×10^{-6}
A2	88.79	-4.99×10^0	1.83×10^{-5}	89.76	-5.074	7.89×10^{-5}
D1	190.41	-5.79×10^{-4}	2.84×10^1	189.81	-1.19×10^{-5}	28.39
D2	190.12	-4.52×10^{-4}	2.84×10^1	189.53	-1.20×10^{-5}	28.36

* Present QUICK scheme; 80×80; ... * * [5]'s spectral multidomain method, 41×41

Some numerical results are briefly presented here. Interested reader may find detailed discussion in reference [8]. Figure 2 gives the streamlines of case **B2**, which typifies the general characteristics observed in group **B**. From the figure, it is fairly obvious that there are two vortices with opposite directions appeared in the upper left corner just under the crystal and the lower right corner. With the increase of rotation speeds of the crystal and crucible, the upper left vortex produced by the crystal rotation moves towards right corner, whereas the lower right vortex induced by the crucible rotation moves to left and dominates the flow field. It is apparent that for possible optimum crystal growth condition requiring only the presence of a single vortical region, both the crystal and crucible cannot be made rotated at the same time

Figure 3 depicts the streamlines of case **C2**, typifying the calculations belonging to group **C**. In this group, the crystal and crucible are at rest and the side wall Grashof number increases from 1.0×10^5 to 1.0×10^7. When Grashof number increases, the vortex gets enlarged and its highest velocity layer moves to the side wall of the crucible. It should be noted that the centre of vortex seems not to change its position at all. Figure 4 shows the contours of temperature for **C2**. It can be seen that when Grashof numer is increased, the contours are compressed towards the centre of crucible, which means that the remaining region of crucible is dominated by the high temperature. In the [2], it was found that when Grashof number reached 10^7, the periodical oscillation occured with numerical solution. However, in the present study no numerical oscillating is found for the Grashof number up to 10^7.

The numerical results of reference [2], which were obtained using central difference scheme, are also listed in the last two columns of Table 3. The comparison between the present results and [2]'s results, except for some [2]'s results for values of ψ_{min} in cases A1 and B1, shows that the present QUICK scheme can solve much higher Grashof number problem with the accuracy as high as the central difference scheme for engineering applications. It should be noted that the present value of ψ_{min} for case A1 is almost the same as [5]'s listed in the Table 2. Unfortunately, there is no available data for further comparison for case B1.

Part Ⅱ. Simulation of Bulk Flows in Horizontal Bridgman Growth on a Centrifuge

One of the main problems in the melt growth techniques is the formation of a spatial type of micro-inhomo-

geneities(Striation)which leads to grown semiconductor single crystals with the defects of non-uniformity. The unsteady buoyancy-driven convection which is present in the melt has been considered to be the most important cause of the melt temperature fluctuation, and ultimately resulting in formation of the doping striation [9]. Recent studies have brought to light the possibility of growing homogeneous crystals with the aid of a centrifuge.

Experiments have been performed using Bridgman method to grow crystals with improved qualities in high gravity conditions by means of centrifuges [10 – 15]. It has been suggested that the Coriolis force, rather than "high gravity", produced by the centrifuge rotation may have a stabilizing influence on unsteady buoyancy convection flows, and leads to the improvement of the quality of growing crystals.

We present here the results of three-dimensional numerical modeling of bulk flows in horizontal Bridgman growth on a centrifuge with various Grashof numbers in time-dependent flow regimes. The important effect of Coriolis force on convection flows is taken into consideration.

Description of the Model

Horizontal Bridgman growth on a centrifuge is schematically depicted in figure 5. A horizontal cylindrical furnace was hung on the end of the arm via a bearing with its axis perpendicular to the centrifuge arm and earth gravity. An open-boat-shaped crucible containing a molten metal was positioned in the furnace. The crucible is considered in this simulation as a rectangular parallelepiped with free surface on the top. The melt is heated by furnace with a horizontal linear temperature gradient, so that the bulk thermal buoyant convection is generated with the flow ascending at hot end and descending at cold end. Figure 6 shows the geometry of the problem. In this study it is assumed that the flow is driven solely by thermal buoyancy force caused by the combined action of horizontal temperature gradient and centrifugal accelerationg. The Marangoni convection is ignored. The centrifugal and Coriolis acceleration effects are separately treated in terms of non-dimensional parameters Gr and Ta (Grashof number and Taylor number), respectively.

The following non-dimensional continuity equation, Navier-Stokes equation with Bossinesq approximation and the energy equation describe the melt flow in the crucible:

$$\nabla \cdot u = 0 \tag{7}$$

$$u_t + (u\cdot\nabla)u = \nabla p + \frac{1}{\sqrt{Gr}}\nabla^2 u + e_g T - \frac{\sqrt{|Ta|}}{\sqrt{Gr}} e_\omega \times u \tag{8}$$

$$T_t + (u\cdot\nabla)T = \frac{1}{Pr\sqrt{Gr}}\nabla^2 T \tag{9}$$

The last two terms in equation(8)are the buoyancy force and Coriolis force, respectively. We use non-dimensioning scale factors length H, time $H^2/(\upsilon\cdot\sqrt{Gr})$, velocity $\upsilon\cdot\sqrt{Gr}/H$ and pressure $\rho\upsilon^2 Gr/H^2$, and the non-dimensional temperature is defined as $(T-T_C)/(T_H-T_C)$. e_g and e_ω refer to the unit vectors in directions of resultant gravity g_r and the rotation velocity vector of the centrifuge ω, respectively. With the assumption of neglecting the effect of earth gravity g_e, e_ω will be parallel to axis z, (see fig.5).

The non-dimensional parameters are Prandtl number $Pr=\upsilon/\kappa$, Grashof number, $Gr=g\beta(T_H-T_C)H^3/\upsilon^2$ and the Taylor number Ta, with $|Ta|=4\omega^2H^4/\upsilon^2$. The Taylor number reflects the relative strength of Coriolis acceleration. Its sign is determined by the centrifuge rotation sense. The negative Ta corresponds to that situation of e_ω is parallel to axis z. (i.e. the centrifuge rotation is in the same sense as the primary convection roll in the melt). The positive Ta corresponds to that e_ω is counter-parallel to axis z. (i.e. both centrifuge rotation and melt convection roll are in the counter direction.)

The following boundary conditions are employed. The no slip condition is applied at all crucible walls. The horizontal free surface is assumed flat and stress-free.

$u = 0$ at boat wall,

$\frac{\partial u}{\partial n} = 0$ at free surface.

The temperatures at two end-walls are fixed at T_C and T_H respectively. Both the sidewall and the free surface are imposed with a fixed linear temperature profile.

Numerical Results and Discussion

The basic equations are solved in three-dimensional and time-dependent form by the finite volume method with PISO algorithm(Pressure Implicit Solution by Spilt Operator method)[16]. The self-filter central differential scheme is employed for variables of velocity and temperature. Since the entire geometry is symmetrical with respect to the central vertical plane, the calculation of the flow field will be undertaken within half domain. A 40x12x10 mush is used in this simulation.

The calculation started from the initial conditions of a static flow field with the temperature $T = 0$ everywhere. To seek the critical state of an oscillatory motion and optimal stabilizing conditions calculations should be repeated for various values of Gr and Ta. In order to compare the existing work the physical parameters of molten GaAs as used in semiconductor devices are adopted.

The time-dependent behavior of the melt flow can be described by the non-dimensional total kinetic energy

$$E = \frac{1}{2}\int_{\Omega}(U^2 + V^2 + W^2)d\Omega \tag{10}$$

Here Ω is the flow domain and U, V, W denote the velocity components. We first computed the non-rotational cases(i.e. with $Ta = 0$ and various Gr). The flow is steady at low Gr. With the increase of Gr, the flow tends to oscillate periodically and the amplitudes increase progressively. At higher Gr it exhibits irregular oscillations, see figure 7. The evolution of the temperature at the central point of the melt is also shown in the figure. One should note that the evolution trends of both E and T are similar. It is found from the calculation that the critical value of Gr whether oscillation will occur is located between 3.7×10^5 and 5.5×10^5. This reasonably agrees with the results of Dupont et al [17] and Oda et al [18].

When the centrifuge is rotating, the Coriolis effect is taken into account. The results have dramatically changed from the case of $Ta = 0$. Figure 8 shows the evolution of the temperature at the melt center and the total kinetic energy of the melt for a given Grashof number, ($Gr = 9 \times 10^5$) and different Taylor numbers, ($Ta = 0$, $Ta = -1 \times 10^4$ and $Ta = 1 \times 10^4$ respectively). It is evidently seen that the oscillation of kinetic energy is totally suppressed for the case of $Ta = -1 \times 10^4$. It is, however, not retarded for the case of $Ta = 1 \times 10^4$. The temperature indicates similar behavior. This implies that the Coriolis force has a sensible influence on the bulk flow in the melt. The most important point is the sign of Ta, (i.e. the rotation direction of the centrifuge) which determines the different actions of Coriolis accelerations upon the convective flows in melt even though the magnitudes of Coriolis accelerations are the same. This result is coincident with the temperature measurement experiment[19], (see figure. 3 of reference[19]).

In addition the simulation results indicate that for a specific Gr the stabilizing effect of Coriolis force only occur at a particular range of Ta, even though Ta is negative. This has not been reported in the experiment of reference[19].

Figure 9 presents the perspective view of velocity vectors and isotherm distributions in various section planes at time = 100 seconds for three cases of figure 4. Convective flow structures with somewhat different features can be observed. Nevertheless as indicated by Dupont et al [20], there is no multicellular pattern found in all vertical section planes which had been calculated for two-dimensional flows[20,21].

Conclusions

A second order QUICK control volume code is developed to simulate the flows in Czochralski crystal growth. As many as 12 cases are calculated to examine the effects of different parameters on the flow behaviour. From the calculations, it can be concluded that the second order upwind QUICK scheme has much more numerical stability and can give very accurate numerical results. Although the present computation is carried out in a rectangular physical region, the present control volume code can be easily adapted for use in the curvilinear coordinate system because of its body-fitted nature.

Three-dimensional and time-dependent numerical simulation for the bulk flow in horizontal Bridgman crystal growth on a centrifuge is carried out. The results show the importance of Coriolis force, which is produced due to the centrifuge rotation, and acts to stabilize the oscillatory motion in the melt. The nature of influence depends on the rotating rate and direction of the centrifuge. This verified the previous observation of model experiments.

Acknowledgements

W. J. Ma wish to express his sincere appreciation to National University of Singapore for providing him the opportunity of visiting stay in the Center for Computational Mechanics, NUS. The work in Part II is partially the research project supported by National Natural Science Foundation of China. The helpful discussions of Dr. C. Shu and Prof. M. L. Xue are gratefully acknowledged.

Tab 4 Some Results for Test Cases by QUICK Scheme and Centre Difference Scheme

Case	Gr	Re_X	Re_C	$\lvert U\rvert^*_{max}$	ψ^*_{min}	ψ^*_{max}	ψ^{**}_{min}	ψ^{**}_{max}
A1	0	10^2	0	4.3682×10^{0}	-2.1724×10^{-1}	4.0630×10^{-6}	-2.3447×10^{1}	1.5642×10^{-6}
A2	0	10^3	0	8.8789×10^{1}	-4.9939×10^{0}	1.8260×10^{-5}	-5.3642×10^{0}	1.5257×10^{-4}
A3	0	10^4	0	9.6105×10^{2}	-4.1168×10^{1}	1.0443×10^{-1}	-4.0443×10^{1}	1.9320×10^{-1}
B1	0	10^2	-25.0	1.9957×10^{0}	-4.4332×10^{-2}	1.1772×10^{-1}	-5.0203×10^{-1}	1.1796×10^{-1}
B2	0	10^3	-250.0	6.5447×10^{1}	-1.4777×10^{0}	1.1480×10^{0}	-1.6835×10^{0}	1.2414×10^{0}
B3	0	10^4	-2500.0	8.2944×10^{2}	-8.7250×10^{0}	5.3881×10^{0}	-8.5415×10^{0}	5.2708×10^{0}
C1	10^5	0	0	1.9041×10^{2}	-5.7979×10^{-4}	2.8409×10^{1}	-1.1936×10^{-3}	2.8437×10^{1}
C2	10^6	0	0	7.1058×10^{2}	-1.1995×10^{-1}	9.2508×10^{1}	-3.9699×10^{-1}	9.2100×10^{1}
C3	10^7	0	0	2.6828×10^{3}	-2.2398×10^{0}	1.8479×10^{2}	not available	not available
D1	10^5	10^1	0	1.9041×10^{2}	-5.7850×10^{-4}	2.8409×10^{1}	-4.7092×10^{-4}	2.8420×10^{1}
D2	10^5	10^2	0	1.9012×10^{2}	-4.5174×10^{-4}	2.8383×10^{1}	-4.7057×10^{-4}	2.8393×10^{1}
D3	10^5	10^3	0	1.6239×10^{2}	-5.6765×10^{-1}	2.5169×10^{1}	-6.5631×10^{-1}	2.4829×10^{1}

* Present QUICK scheme with 80×80 grid * * [2]'s central difference scheme with 64×64 grid.

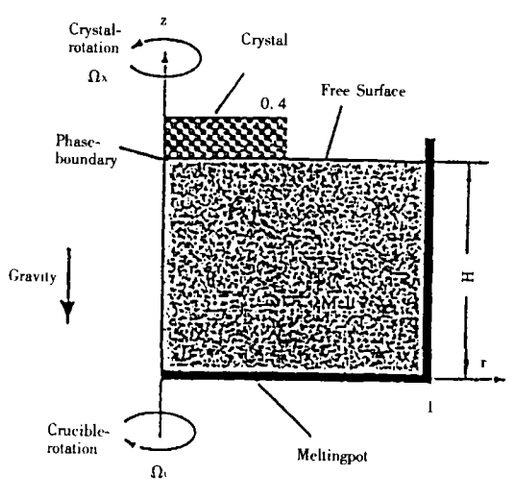

Fig. 1 The configuration of Czochralski crystal growth

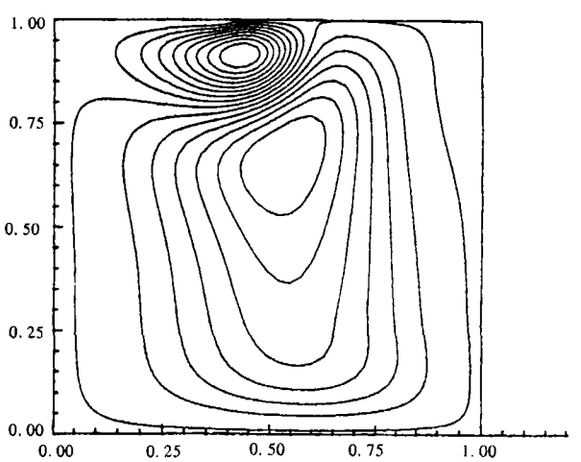

Fig. 2 Streamlines of case B2, Gr = 0.0, $Re_X = 10^2$, $Re_C = -2.5\times10^2$.

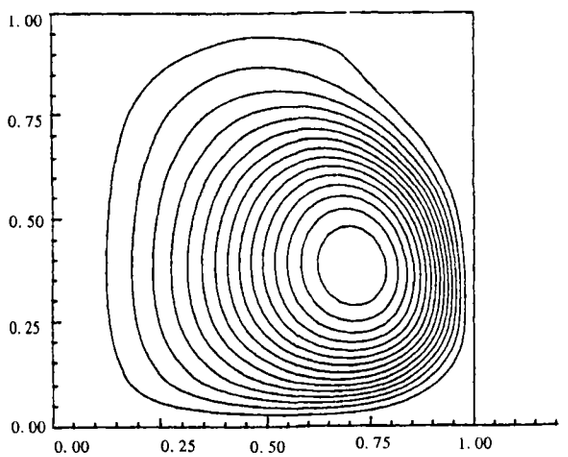

Fig.3 Streamlines of case C2, $Gr = 10^6$, $Re_X = 0.0$, $Re_C = 0.0$

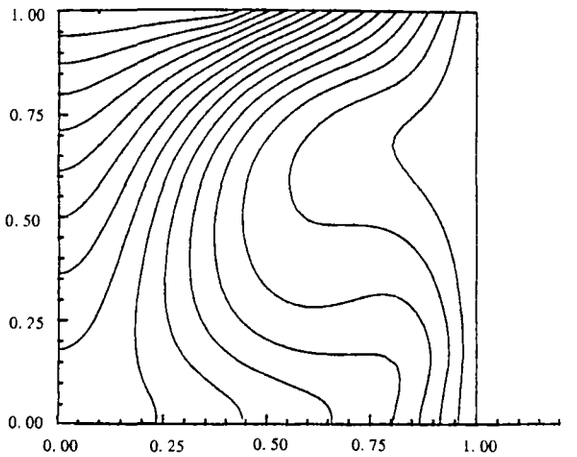

Fig.4 Temperature of case C2, $Gr = 10^6$, $Re_X = 0.0$, $Re_C = 0.0$

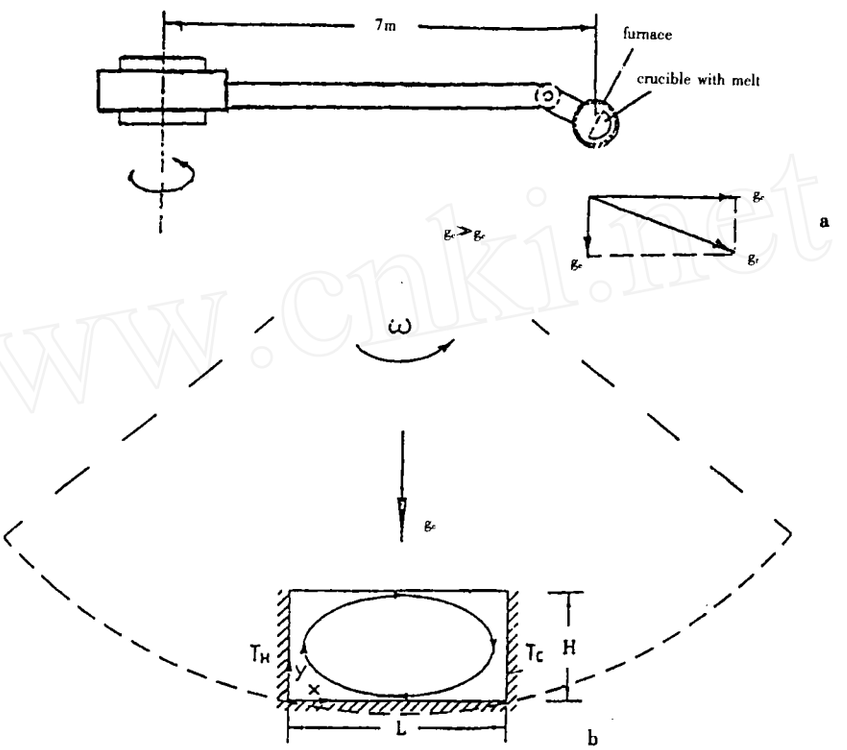

Fig.5 Sketch of crystal growth by the horizontal Bridgman technique on a large centrifuge(a), Schematic illustration of the top view, the crucible is simplified as a rectangular parallelepiped with enlarged size to show the inside flow(b).

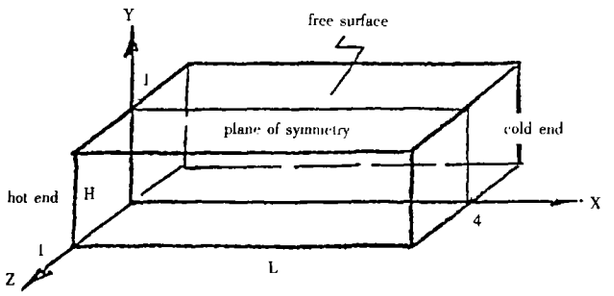

Fig.6 Geometry of the problem

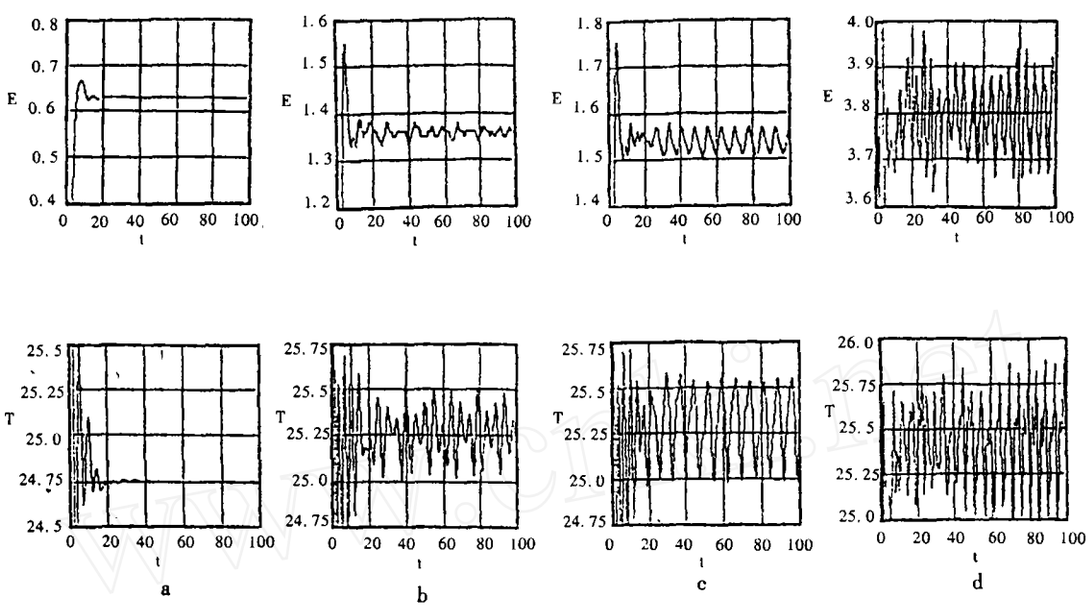

Fig.7 The non-dimensional total kinetic energy E (10^6) and temperature T (℃) at the melt center versus time t (sec) for Taylor number Ta = 0 and various Grashof numbers: (a) Gr = 3.7×10^5, (b) Gr = 8×10^5, (c) Gr = 9×10^5, (d) Gr = 2×10^6

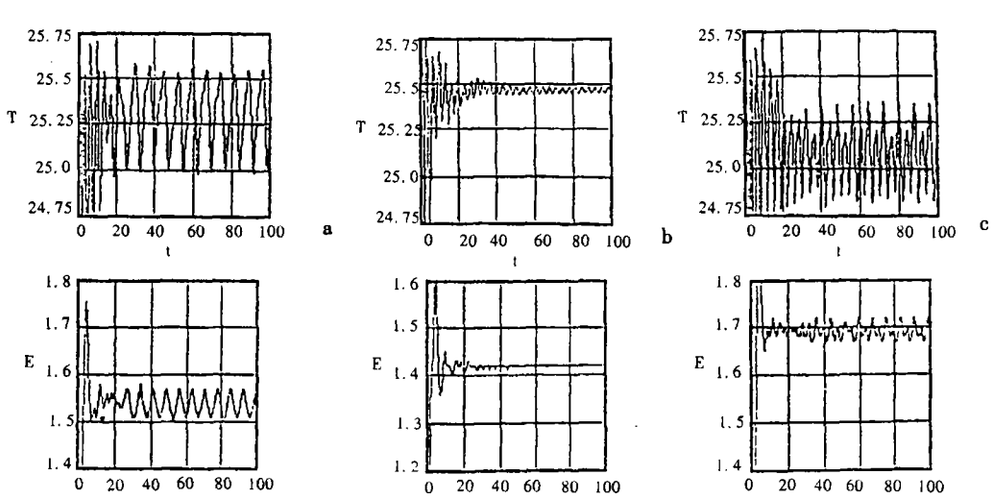

Fig.8 The temperature T(℃) at the melt center and the non-dimensional total kinetic energy E(10^6) versus time t (sec) for Grashof number Gr = 9×10^5 and various Taylor numbers Ta: (a) Ta = 0, (b) Ta = -1×10^4 (c) Ta = 1×10^4

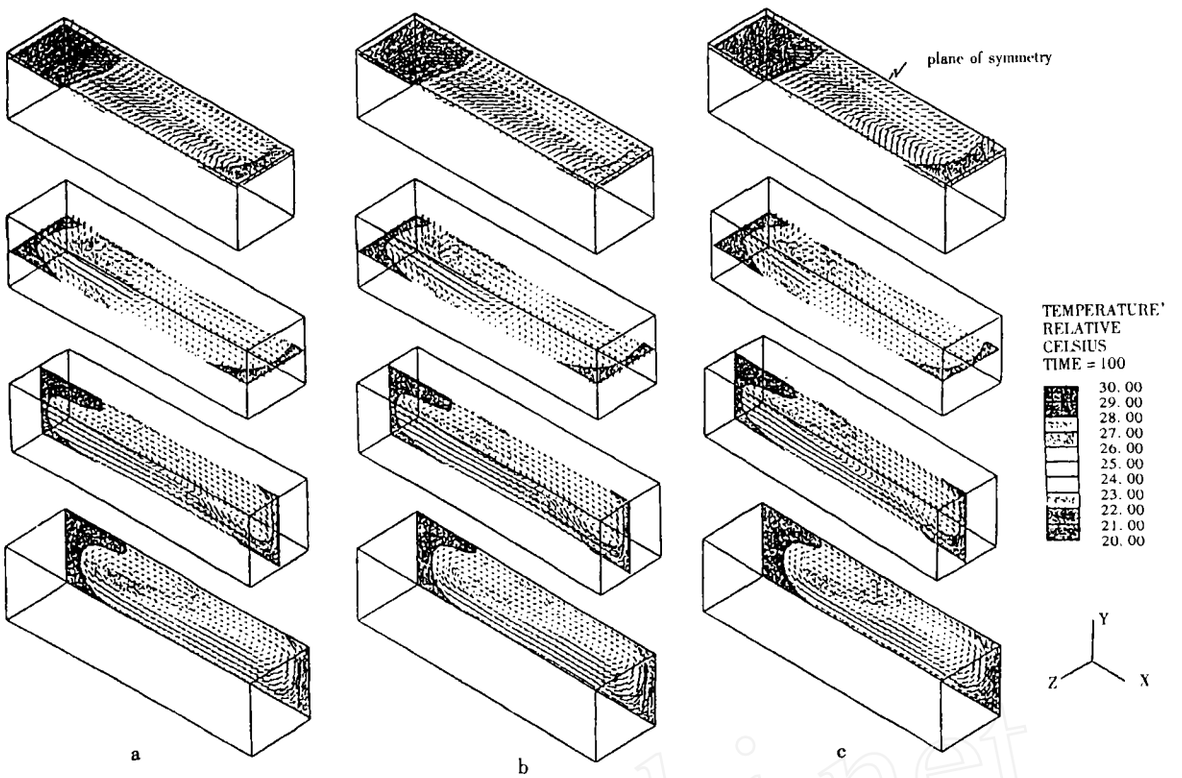

Fig.9 Perspective view of velocity vectors and isotherm distributions in various section planes for three cases of fig.4 a, b and c.

Reference

[1] W.E. Langlois. Buoyancy Driven Flows in Crystal Growth Melts, Ann. Rev. Fluid. Mech. 1985, 17:191~215.

[2] U. Buckle and M. Schafer. Benchmark results for the numerical simulation of flow in Czochralski crystal growth, J. of Crystal Growth, 1993, 126: 682~694.

[3] J.R. Ristorcelli and J.L. Lumley. A second order turbulence simulation of the Czochralski crystal growth melt: the buoyantly driven flow, J. of Crystal Growth, 1993, 129:249~265.

[4] Q. Xiao and J.J. Derby. Heat transfer and interface inversion during the Czochralski growth of yttrium aluminum garnet and gadolinium garnet, J. of Crystal Growth, 1994, 139:147~157.

[5] I. Paspo, J. Ouazzani and R. Peyret. A spectral multidomain technique for the computation of the Czochralski melt configuration, Int. J. Num. Meth. Heat Fluid Flow, 1998, 6:31~58.

[6] A.A. Wheeler. J. Crystal Growth, 1990, 102:691.

[7] P.G. Huang and M.A. Leschziner. An introduction and guide to the computer code TEAM-Preliminary version, Flair, UMIST, July 1983.

[8] D. Xu, C. Shu and B.C. Khoo. Numerical simulation of flows in Czochralski crystal growth by second-order upwind QUICK scheme, J. of Crystal Growth, 1997, 173:123~131.

[9] G. Muller. Convection and Inhomogeneities in: Crystal Growth from the melt, Crystals Vol. 12(Springer, Berlin, 1988).

[10] H. Rodot, L.L. Regel, G.V. Sarafanov, H. Hamidi, I.V. Videskii and A.M. Turtchaninov. J. Crystal Growth, 1986, 79:77.

[11] H. Rodot, L.L. Regel and A.M. Turtchaninov. J. Crystal Growth, 1990, 104:280.

[12] G. Muller, P. Kyr and E. Schmidt. J. Crystal Growth, 1980, 49:387.

[13] G. Muller, G. Neumann. J. Crystal Growth, 1982, 59:548.

[14] X.R. Zhong, B.J. Zhou, Q.M. >Yan, F.N. Cao, C.J. Li, L.Y. Lin and W.J. Ma, Y. Zheng, F. Tao, M.L. Xue. J. Crystal Growth, 1992, 119: 74.

[15] B.J. Zhou, F.N. Cao, L.Y. Lin and W.J. Ma, Y. Zheng, F. Tao, M.L. Xue. Growth of GaAs single crystals under high gravity condition, in: Materials Processing in High Gravity, Ed. by L.L. Regel and W.R. Wilcox. Plenum. New York, 1994, 53.

[16] R.I. Issa, A.d. Gosman and A.P. Watkins. J. Comp. Phys., 1986, 62:66.

[17] S. Dupont and J.M. Marchal. Int. J. Numerical Methods in Fluids, 1988, 8:183.

[18] K. Oda, T. Saito. J. Nishihama and T. Ishihara, J. Crystal Growth, 1989, 97:186.

[19] W.J. Ma, F. Tao, Y. Zheng, M.L. Xue, B.J. Zhou and L.Y. Lin. Response of temperature oscillations in a tin melt to Centrifugal effects, in Materials Processing in High Gravity, Ed. by L.L. Regel and W.R. Wilcox. New York: Plenum Press, 1994, 61.

[20] S. Dupont, J.M. Marchal and M.J. Crochet. Int. J. Numerical Methods in Fluids, 1987, 7:49.

[21] F. Tao, Y. Zheng, W.J. Ma and M.L. Xue. Unsteady thermal convection of melts in a 2-D horizontal boat in a centrifugal field with consideration of Coriolis effect, in Materials Processing in High Gravity, Ed. by L.L. Regel and W.R. Wilcox, New York: Plenum Press, 1994, 67.

熔液法晶体生长流场的数值模拟

博士、高级讲师、研究中心副主任　邱武昌
（新加坡国立大学计算力学中心）
博士后、高级研究工程师　徐　雕
（新加坡国立大学计算力学中心）
副研究员、访问学者　马文驹
（中国科学院力学研究所；新加坡国立大学）

提　要：本文给出了对二种熔液法生长晶体的液相流场进行的计算机模拟的结果，对 CZ 法晶体生长的定常流场数值计算，采用了二阶迎风 QUICK 差分格式的有限控制体积法，通过对 12 种不同参数的流场情况所作的计算表明，二阶 QUICK 格式具有更高的计算精度和数值稳定性。对离心机环境下的水平 Bridgman 晶体生长的流场进行了三维非定常的数值模拟。结果表明，在一定的旋转方向和旋转速率条件下，离心机环境中的 Coriolis 力对熔体振荡流动有致稳作用。计算结果符合以往实验的发现，并优于二维非定常模拟结果。

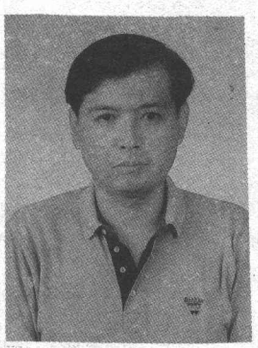

作者简介

邱武昌（B. C. Khoo）。邱武昌 1980 年获英国剑桥大学工学学士荣誉学位，同年又获该校皇家航空奖，1984 年获新加坡国立大学硕士学位，1989 年获美国麻省理工学院工学博士学位，现任新加坡国立大学机械与制造工程系高级讲师和该校计算力学中心副主任。具有多方面科研兴趣。在国际期刊与国际会议上发表 90 多篇论文。

徐　雕（D.Xu）。徐雕 1982 年获西安交通大学工学学士学位，1985 年获该校工学硕士学位。1988 年获南京航空航天大学工学博士学位后，在该校任教和从事流体力学和流体机械方面研究。1994 年获英国皇家学会资助，在曼彻斯特理工大学（UMIST）机械系从事博士后科研工作。1996 年到新加坡国立大学计算力学中心任高级研究工程师。从事流体力学和流体机械方面研究。主要研究领域有：叶片机空气动力学，计算流体动力学，紊流流动数值模拟和熔液法晶体生长数值模拟等。

马文驹（W. J. Ma）。马文驹 1966 年中国科技大学力学系流体力学专业毕业，毕业后在中国科学院力学研究所先后从事高超音速绕流场的数值计算，高超音速气动力学和气动物理实验及混合层内大涡拟序结构研究，1983—1984 年作为访问学者在日本理化学研究所从事自然对流课题的合作研究，1988 年起为中国科学院力学研究所副研究员，开始进行晶体生长中流体力学问题和超重力环境下材料制备的研究工作，参加并主持了有关这方面的国家自然科学基金项目的研究。现应邀在新加坡国立大学作访问学者。

（责任编辑：许　蓉）